Biomaterials 97 (2016) 164–175

Contents lists available at ScienceDirect

Biomaterials

journal homepage: www.elsevier.com/locate/biomaterials

Human relaxin gene expression delivered by bioreducible dendrimer polymer for post-infarct cardiac remodeling in rats

Young Sook Lee [a], Joung-Woo Choi [a], Jung-Eun Oh [b], Chae-Ok Yun [b, *], Sung Wan Kim [a, b]

[a] Center for Controlled Chemical Delivery, Department of Pharmaceutics and Pharmaceutical Chemistry, University of Utah, Salt Lake City, UT, 84112, USA
[b] Department of Bioengineering, College of Engineering, Hanyang University, 222 Wangsimni-ro, Seongdong-gu, Seoul, 133-791, Republic of Korea

ARTICLE INFO

Article history:
Received 12 January 2016
Received in revised form
12 April 2016
Accepted 21 April 2016
Available online 26 April 2016

Keywords:
Relaxin gene therapy
Myocardial infarction
Bioreducible polymer
Dendrimer
Cardiac extracellular matrix (ECM)
Post-infarct remodeling
Infarct-related coronary artery

ABSTRACT

In consensus, myocardial infarction (MI) is defined as irreversible cell death secondary to prolonged ischemia in heart. The aim of our study was to evaluate the therapeutic potential of anti-fibrotic human Relaxin-expressing plasmid DNA with hypoxia response element (HRE) 12 copies (*HR1*) delivered by a dendrimer type PAM-ABP polymer G0 (*HR1*/G0) after MI on functional, hemodynamic, geometric, and cardiac extracellular matrix (ECM) remodeling in rats. *HR1*/G0 demonstrated significantly improved LV systolic function, hemodynamic parameters, and geometry on 1 wk and 4 wks after MI in rats, compared with I/R group. The resolution of regional wall motional abnormalities and the increased blood flow of infarct-related coronary artery supported functional improvements of *HR1*/G0. Furthermore, *HR1*/G0 polyplex showed favorable post-infarct cardiac ECM remodeling reflected on the favorable cardiac ECM compositions. Overall, this is the first study, which presented an advanced platform for the gene therapy that reverses adverse cardiac remodeling after MI with a *HR1* gene delivered by a bioreducible dendrimer polymer in the cardiac ECM.

1. Introduction

MI caused by occlusion of coronary artery is the leading cause of mortality and morbidity in the world [1–7]. It is predicted that the direct medical costs of all cardiovascular diseases, including hypertension, coronary artery disease (CAD), heart failure (HF), and stroke will triple, reaching $818 billion in 2030 [8]. The percutaneous coronary intervention (PCI), restoring blood flow to the ischemic myocardium reduces infarct size by 40%. Without reperfusion by PCI, the infarct size in heart reaches about 70% [3]. Therefore, myocardial ischemia/reperfusion (I/R) injury followed by PCI causes the unrescued part of remaining 30% infarct and partially explains 10% of mortality and 25% of heart failure after MI despite optimal myocardial reperfusion [3,9]. This unrescued myocardium followed by I/R injury can be restored by several futural cardioprotective strategies. The post-infarct cardiac remodeling undergoes sequential features in inflammatory, proliferative, and healing phases [10–12]. A final common pathologic hallmark of cardiac remodeling is fibrosis by excessive deposition of extracellular matrix (ECM) components, which causes systolic and diastolic dysfunction, rhythm disturbances, morbidity, and mortality [12–18]. The compositional changes in ECM is not a passive by-product, but an active player in the cellular and extracellular events in diseases, especially determining fibrosis [18]. Although the cardioprotective effects of therapeutic genes within the ischemic myocardium has had some success as a MI treatment, its promise has been limited because of not recovering the central fibrotic scar lesion in heart tissues [1]. Even if fibrosis is a leading cause of organ failure in diverse diseases, no effective treatment strategies exist [12,19–21]. Reversal of cardiac fibrosis toward favorable cardiac ECM remodeling is one of ultimate aims to preserve heart function after MI [17].

Gender-related differences in cardiovascular disease (CVD), especially the lower incidence of CVD in pre-menopausal women have been chiefly related to protective ovarian steroids. However, estrogen or progesterone have not been clearly identified as the protective agents in women and are still controversial. In addition to steroids, the ovary also produces the peptide hormone relaxin (RLX), which was first identified for its role in reproduction and pregnancy by Frederick Hisaw in 1926 [22,23]. Recently, RLX, a pleiotropic hormone has been shown to have a wide range of biologic actions, including anti-inflammatory, antiapoptotic, positive

* Corresponding author.
E-mail address: chaeok@hanyang.ac.kr (C.-O. Yun).
URL: http://hanyang-genetherapylab.co.kr

http://dx.doi.org/10.1016/j.biomaterials.2016.04.025
0142-9612/

chronotropic and inotropic, vasodilatory, antiarrhythmic, antifibrotic, and proangiogenic effects [17,24–29]. There are some studies of recombinant human RLX protein (rhRLX) to investigate effects on the myocardial infarction and cardiomyopathy [29–31]. Serelaxin, a recombinant protein of human RLX2 is ongoing phase III clinical trial for patients with acute HF [25,32,33]. Diverse potent cardioprotective effects of RLX render it one of the most likely candidates for the elusive physiological shield against CVD, including MI.

The extracellular matrix (ECM) in the heart, which is filled with negatively charged proteoglycans and glycosaminoglycans such as hyaluronan, has been considered as a hurdle in gene therapy. Therefore, most researchers have been circumventing this problem with neutrally charged particles and plasmid DNA or RNA itself. Moreover, we do not yet understand the precise cellular and molecular mechanisms necessary to produce an ECM that is sufficient for tissue strength and elasticity without excessive deposition of fibrous proteins such as collagen. Dendrimers are versatile and derivatisable chemical polymers, which can be modified into biocompatible compounds with low cytotoxicity and high biopermeability [34–37]. The cationic, amino-terminated dendrimers can exhibit long-term retention in the ECM giving a very high local concentration of the carried substrate and acting as a drug depot at the cellular surface [34–40]. To accomplish the prominent therapeutic effects of gene delivery in post-infarct cardiac remodeling, a cardioprotective gene focused on cardiac ECM remodeling, which exhibits targeted and prolonged accumulation in ischemic myocardium as well as protects against an adverse post-infarct cardiac remodeling, is needed.

Here, we utilized a dendrimer type PAM-ABP polymer [41], retaining the unique properties of reductive disulfide linkers coupled with the advantage of arginine residues to enhance cell penetration and exhibiting long-term retention in the ECM, giving a high local concentration of the carried therapeutic gene and acting as a drug depot at the cellular surface. We were able to enhance the *in vitro* transfection efficacy of *HR1* both under hypoxia as well as under normoxia. Furthermore, we explored the remarkable effects of *HR1* delivered by a dendrimer type PAM-ABP G0 polymer (*HR1*/G0) on systolic and hemodynamic function, geometry, and cardiac ECM derangement during post-infarct cardiac remodeling in rats. Lastly, the *HR1*/G0 delivery system augmented the myocardial perfusion by coronary artery in a coordinated way eventually to rescue the function of infarcted myocardium in rats.

2. Materials and methods

2.1. Materials preparation

2.1.1. Construction of HR1

The human Relaxin 1-expressing plasmid DNA (*R1*) and 12 copies of hypoxia-response element (HRE) plasmid DNA (*pDNA*) were transferred from Hanyang University. Two plasmid DNA of *R1* and HRE 12 copies were confirmed by gene sequencing. The *R1* (942 bp) was inserted into pcDNA3.1(-) (5427 bp, Invitrogen) using the enzyme restriction of BamH I and Hind III. Then, the HRE12 insert (600 bp) restricted by the EcoR I was ligated into Mfe I site. Finally, the *R1* with HRE 12 copies (abbreviated as a *HR1*, Suppl. Fig. 1) was confirmed in the electrophoresis with expected sizes followed by the different enzyme restrictions.

2.1.2. Selection and preparation of HR1/polymer polyplexes

We purified the pCMV-*HR1* DNA as previously described [42]. *HR1* and *GFP pDNA* (gWiz-GFP, Aldevron) were purified with an endotoxin-free plasmid DNA purification NucleoBond® Xtra Maxi plus EF kit (Macherey-Nagel Inc.). The arginine-grafted bioreducible poly(disulfide amine) (ABP) polymer, generation 0 (G0), and G1 ABP-conjugated polyamidoamine (PAMAM) dendrimer (PAM-ABP) were synthesized as previously described [41,43,44]. ABP was incorporated into the poly(amido-amine) (PAMAM) dendrimer, creating a high molecular weight bio-reducible polymer, PAM-ABP. G0 PAM-ABP was composed of a backbone of PAMAM G0 and four ABP residues at the surface. Then, G1 PAM-ABP had eight ABP residues (Suppl. Fig. 2). The *HR1* plasmid DNA–alone and branched poly(ethylenimine) (bPEI, 25 kDa, Sigma-Aldrich) polyplex (*HR1*/PEI) were used as controls. The *HR1* polyplexes were prepared in a 20 mM HEPES/5% glucose buffer. After incubation for 30 min at room temperature, the particle size of the polyplex samples was evaluated by dynamic light scattering using a Zetasizer Nano ZS (Malvern Instruments Ltd.). Surface charge was measured by determination of Zeta potential using the same instrument.

2.2. In vitro cell experiment

2.2.1. Transfection efficiency

The H9C2 cells, rat myoblast cell line, were maintained in Dulbecco's Modified Eagle's Medium (DMEM) containing 10% fetal bovine serum (FBS) and 1% antibiotics at 37 °C under 5% CO_2. At 80% confluence, the cells were seeded on 24-well plates at a density of 5×10^4 cells/well. After 24 h of incubation, the culture media were replaced with fresh DMEM containing *pDNA*/polymer polyplexes prepared by mixing 1 μg *pDNA* and wt ratio of polymer. After 4 h, the cells were washed with phosphate buffered saline (PBS) and cultured with DMEM containing 10% FBS. To evaluate the transfection efficiency under the hypoxia condition, the 24-well culture plates were placed in a hypoxia chamber filled with mixed gas composed of 5% CO_2, 1% O_2, and 94% N_2. After 48 h, the GFP expression was quantified in the microplate reader (Tecan infinite M200® Pro) with images under the light microscope. The amount of RLX production and total protein were determined using a Relaxin ELISA kit (R&D Systems) and BCA assay kit (Pierce), respectively, according to the manufacturers' protocols. The cells were lysed with 150 μl of lysis buffer containing a protease & phosphatase inhibitor cocktail (Sigma). The cells were harvested and centrifuged for 30 s at 13,000 rpm.

2.2.2. In vitro cellular uptake assay and scratch assay

In H9C2 cells, YOYO-1 iodide– (1 mmol/L in DMSO; Molecular Probes) tagged *HR1* (1 molecule dye per 50 bp nucleotide) was prepared in the dark for 30 min. Polyplexes were prepared by mixing YOYO-1 iodide-labeled *HR1* (0.5 μg) with three different ABP, G0, and G1 PAM-ABP polymer at wt/wt ratios of 1/20, 1/5, and 1/5, respectively in 20 mM HEPES/5% glucose solution and incubated at room temperature for 30 min before transfection. *HR1*/PEI (wt/wt 1/1) was used as a positive control. The polyplexes were incubated with cells at 37 °C for 4 h in serum-free media. Samples were analyzed by flow cytometry (FACS Caliber; BD Biosciences) at a minimum of 1×10^4 cells using the FL1 channel for YOYO-1 dye. Untreated cells were used as a negative control for calibration. Cellular uptake (%) was gated on the M1 region and the mean Fluorescence Intensity (MFI) of each group was recorded. Data were analyzed using Windows Multiple Document Interface Software, version 2.9 (WinMDI; Microsoft).

To measure cell migration *in vitro*, NIH3T3 cells, the mouse embryonic fibroblast cell line, were cultured to confluence (>90%) in 6-well plates. After creation of one new artificial gap, scratch using a sterile pipet tip on the bottom of the plates, *R1* and *HR1* alone, *R1*/G0 and *HR1*/G0 at the weight ratio of 1:5, and *HR1*/PEI at the weight ratio of 1:1 were added in serum-free DMEM media. After the 4 h transfection, plates were gently rinsed with PBS and

changed into 10% FBS containing DMEM. The time-dependent light microscopic images were taken until new cell–cell contacts are established again [45].

2.3. Animal study

2.3.1. 3-Dimensional (3D) scanning confocal microscopy of LV

To image the arrangement of structures in cardiac tissue on 1 wk after IR injury and normal rats, heart was harvested in rats. Cardiac myocytes in rats were labeled using wheat germ agglutinin (WGA), which labels glycoconjugates of cell membranes and extracellular matrix (ECM) constituents, demarcating interstitial space. After incubated overnight at 4 °C, the harvested samples of rat heart tissue were washed and stored in PBS solution. The 3D image stacks of labeled cells immersed in glycerol were acquired, using a confocal microscope (LSM 5 Live Duo, Carl Zeiss) equipped with a 63X oil immersion lens (Numeric aperture, 1.4) as described previously [46,47].

2.3.2. MI in rats

We purchased male Sprague-Dawley (SD) rats from Charles River Laboratories at 7–8 weeks-old with a body weight of 220–250 g. All rats were housed in the University of Utah under the Association for Assessment and Accreditation of Laboratory Animal Care International (AAALAC) guidelines. All experiments were approved by the University of Utah Institutional Animal Care and Use Committee and followed the guidelines provided by the National Institutes of Health in *Guide for the Care and Use of Laboratory Animals*. All rats had access to food and water *ad libitum* and were housed in plastic cages on standard 12/12 h light/dark cycles. MI was induced in male SD rats by 30 min surgical occlusion of the left anterior descending (LAD) coronary artery as previously described [1]. The rats were randomly assigned to the one of five groups (each n = 9): 1) sham thoracotomy, 2) I/R only, 3) 200 μg *HR1* alone, 4) 100 μg *HR1*/G0 polyplex (wt/wt = 1: 5), and 5) 200 μg *HR1*/PEI (wt/wt = 1: 1) polyplex. Right after successful ischemia–reperfusion (I/R), the rats received a total injection volume of 100 μl delivered to five separate intramyocardial sites with three injections to the ischemic border zone of the infarct in LV (LVb) and two injections to the central fibrotic zone of the infarct in LV (LVf) with 28 1/2 gauze needle. Animals were followed for 4 weeks after intramyocardial administrations.

2.3.3. Echocardiography

To assess LV function and remodeling in rats, transthoracic echocardiography (TTE) was performed at weeks 1 and 4 after the intramyocardial administration in rats lightly anesthetized with isoflurane at 1–2 L/min and spontaneous respiration. Echocardiograms were performed with a small animal echocardiography system (Vevo2100® High-Resolution Imaging System, VisualSonics Inc.) equipped with a 13- to 24-MHz linear-array transducer (MS250, MS400 MicroScan Transducer, VisualSonics). The ejection fraction (EF, %) was evaluated using the Speckle Tracking Echocardiography (STE) technique. In TTE, time-to-peak analysis displays the synchronicity and phase for different segments of the heart. The phase measures the synchronicity located between regions of the heart for a selected time interval and provides parameters of regional wall motion abnormality (RWMA). As a method of analysis, the phase in this case is defined as the first fundamental Fourier harmonic, each one of the curves is compared to the average curve, and expressed in time delay and percentage of heartbeats.

Transthoracic coronary blood flow velocity and diameter in the proximal LAD (pLAD) coronary artery, infarct-related coronary artery, were measured during diastole and systole on 1 and 4 weeks after post-infarct intramyocardial injections. The transducer was carefully tilted and rotated, using a color doppler image as a guide, until the diastolic coronary blood flow in the LV wall is visualized. Following identification, coronary blood flow velocity was measured by a pulsed wave Doppler technique [48]. All measurements were averaged for 3 consecutive cardiac cycles.

2.3.4. Pathological analysis

Serial 4 μm-thick sections of rat myocardium were fixed, embedded, and stained with hematoxylin and eosin (H&E) stain. Collagen contents were evaluated by Masson's trichrome stain. Immunohistochemical (IHC) staining was performed on the 4 μm-thick sections of formalin-fixed, paraffin-embedded rat hearts tissue. Sections were air-dried at room temperature and then placed in a 60 °C oven for 30 min to melt the paraffin. Slides were deparaffinized in xylene and then hydrated by incubation in a graded series of alcohols. Endogenous peroxidase activity in the sections was blocked with 3% hydrogen peroxide, and slides were blocked with Protein Block Serum-Free (DAKO, Glostrup, Denmark) for 20 min at room temperature. To evaluate the changes of cardiac ECM composition, heart sections were stained using collagen I (1:100 dilution; Abcam, Cambridge, UK), collagen III (1:100 dilution; Abcam, Cambridge, UK), fibronectin (1:50 dilution; Santa Cruz Biotechnology), elastin (1:100 dilution; Sigma-Aldrich) specific antibody in antibody diluents (DAKO, Glostrup, Denmark). After incubating with primary antibodies at 4 °C overnight, the sections were washed twice in PBS and incubated with goat anti-mouse IgG (H + L)-HRP (Southern Biotech) for 2 h at room temperature. Diaminobenzidine/hydrogen peroxidase (DAKO, Carpinteria, CA, USA) was used as the chromogen substrate. The sections were detected using the ULTRAView DAB detection kit (Ventana Medical Systems). The sections were counterstained with Mayer's hematoxylin for 8 min. Analysis of all images was randomly chosen within the infarct border zone of LV and carried out in five random high-power fields per section using the microscope (Carl Zeiss, Jena, Germany; Axioskop 40) (original magnifications = ×400). Expression levels of collagen- I, -III, fibronectin, and elastin were semi-quantitatively analyzed using MetaMorph® image analysis software (Universal Image Corp., Buckinghamshire, UK). Results are expressed as the mean optical density for five different digital images. Data were analyzed by one-way ANOVA.

2.4. Statistical analysis

All data were expressed as mean ± SEM. Comparisons between multiple groups were performed by analysis of variance (ANOVA) followed by Tukey *post-hoc* testing. A p value < 0.05 was considered statistically significant.

3. Results

3.1. In vitro transfection efficacy of HR1

Hypoxia is one of main pathologic characteristics of ischemic heart disease, MI [49]. In the consideration of hypoxia in the post-infarct I/R injury, we modified the human Relaxin 1 plasmid DNA (*R1*) with 12 copies of hypoxia-responsive element (HRE), generating a *HR1* (Suppl. Fig. 1). Recently, we generated new bioreducible polymers; ABP, G0 and G1 PAM-ABP (Suppl. Fig. 2) [41,43]. To select the optimal wt:wt ratio of *pDNA* delivered by different bioreducible polymers, *in vitro* transfection efficacy and cell cytotoxicity of *pGFP* polyplexes were evaluated in H9C2 and C2C12 cells (Fig. 1a). We decided that the optimal wt:wt ratio of ABP/*pGFP* was 20 and G0/*pGFP* and G1/*pGFP* were 5, which fulfill conditions both of higher transfection efficacy and of lower cytotoxicity *in vitro*. Then, the

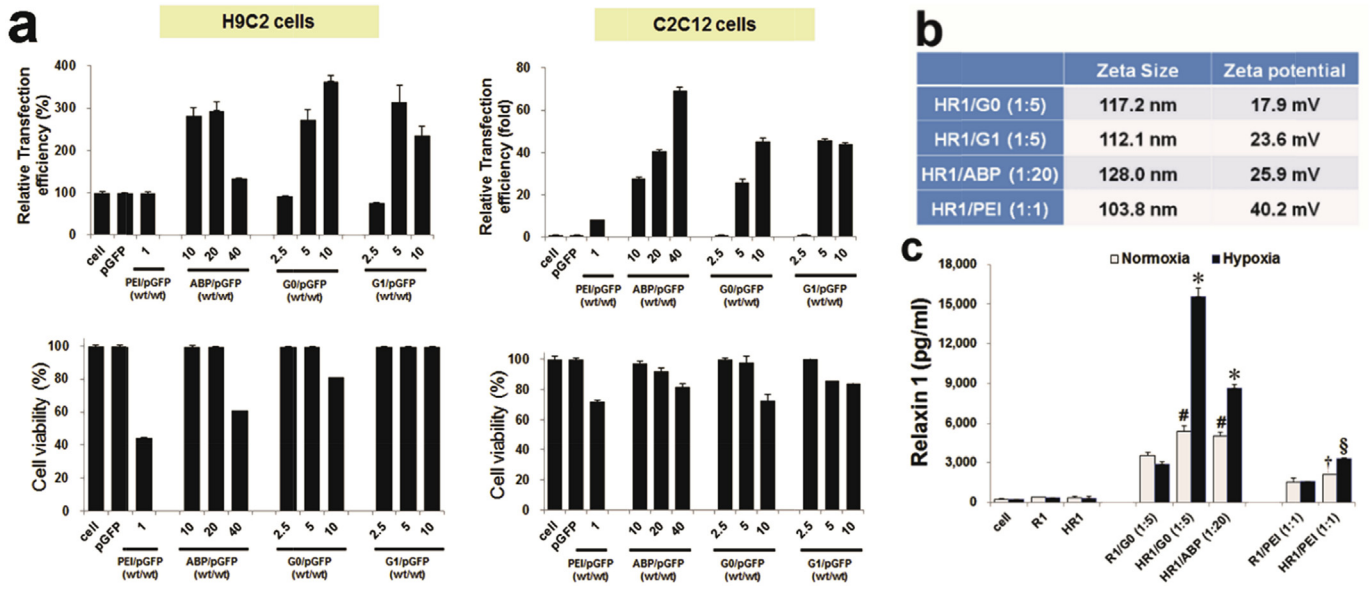

Fig. 1. (a) *In vitro* transfection efficacy and cell cytotoxicity of *pGFP* polyplexes in H9C2 and C2C12 cells. (b) average size and Zeta potential in the optimal wt:wt ratio of *HR1*/polymer polyplexes. (c) comparison of *in vitro* transfection efficacy under hypoxia and normoxia. #$P < 0.05$ vs *R1*/G0 polyplexes under normoxia, *$P < 0.05$ vs *R1*/G0 polyplexes under hypoxia, †$P < 0.05$ vs *R1*/PEI polyplexes under normoxia, and §$P < 0.05$ vs *R1*/PEI polyplexes under hypoxia.

average size and Zeta potential in the optimal wt:wt ratio of *HR1*/polymer polyplexes were measured, along with *HR1*/PEI polyplexes as a positive control (Fig. 1b). Under the hypoxia condition, the effect of insertion of 12 copies of HRE (HRE12) demonstrated 5.3-times higher transfection efficiency in *HR1*/G0, 3.0-times higher in *HR1*/ABP, and 2.1-times higher in *HR1*/PEI polyplexes than respective *R1*/polymer polyplexes (Fig. 1c), implying that the addition of HRE enhances the gene expression in response to hypoxia condition. Interestingly, the incorporation of HRE12 showed 1.4–1.5 times higher transfection efficiency under the normoxia condition than respective *R1*/polymer polyplexes (Fig. 1c).

The *in vitro* cellular uptake by flow cytometry didn't show any significant differences in between ABP, G0, and G1 PAM-ABP polyplexes groups (data not shown). To achieve efficient gene transfection, the cellular uptake is one of major barriers to overcome. Our three bioreducible polymers have a common backbone of ABP residues. ABP had arginine residues as a cell-penetrating peptide, facilitating the enhanced cellular uptake. Our *in vitro* result suggest that the difference in transfection efficacy among three bioreducible polymers is not attributed to their different cell penetrating abilities.

The *in vitro* scratch migration assay is appropriate to evaluate the regulation of cell migration mediated by cell interaction with ECM and cell–cell interactions [45]. Compared with *R1*, *HR1* alone, and *HR1*/PEI polyplex, both *R1*/G0 and *HR1*/G0 at the weight ratio of 1:5 revealed the faster cell migration *in vitro* (Fig. 2). We can speculate that the G0 PAM-ABP delivery system supports higher cell migration under the cell interaction with ECM.

3.2. Ex vivo 3D tissue imaging of HR1/G0

Recent methodology of three-dimensional (3D) scanning confocal microscopy in heart provides quantitative tissue characterization as well as reconstruction of tissue micro-structure based on fluorescent tissue labeling [47]. The side-to-side slippage of myocytes has been observed in the myocardium on 2 days after MI [50]. We evaluated the post-infarct micro-structural changes between in normal myocardium and in infarcted myocardium using the 3D scanning confocal *ex vivo* images with WGA labeling. The central fibrotic zone of LV infarct showed aggressive destruction of alignments of myocytes on 1 wk after IR injury, compared with the border zone of LV infarct as well as normal heart tissue (Fig. 3A). Next, the *in vivo* distribution pattern of different polymeric delivery systems in the frozen sections of rat heart tissues was observed 48 h after intramyocardial injections of *pGFP* polyplexes. The intramyocardial injections of *pGFP*/PAM-ABP G0 polyplexes showed relatively higher homogenous expression of GFP *in vivo* compared with *pGFP* alone and *pGFP*/PEI polyplexes (Fig. 3B). This result suggests that G0 dendrimer delivery system is able to provide wider distribution and increased *in vivo* efficacy of gene therapeutics.

3.3. HR1 delivery improves LV systolic function and cardiac hemodynamic function

The left ventricular ejection fraction (LV EF, %) is a representative functional and prognostic marker in heart [1]. At first, we investigated the time-dependent effects of intramyocardial *HR1*/G0 polyplex injections on the cardiac systolic function and geometry during post-infarct cardiac remodeling using transthoracic echocardiography, compared with other treatment groups in rats. On 1 wk after MI, the 100 μg *HR1*/G0 polyplex (wt:wt = 1:5) group showed about a 15% increase of LV EF than I/R group, even up to the comparable level of sham thoracotomy group (Fig. 4A).

Recent advance in 2D speckle-tracking echocardiography (STE), especially using the analysis of strain and strain rate (SR) analysis provides valuable information especially about the quantification of regional and global myocardial dysfunction (dyssynchrony), assessment of myocardial viability, valuable prognostic information, and the follow-up of treatment response [51]. Strain, like regional ejection fraction is a measure of tissue deformation. SR, a parameter which reflects contractility and is correlated with the rate of change in pressure (dP/dt), measures the time course of deformation [51]. Strain rate imaging (SRI) has provided a valuable physiological tool for understanding myocardial mechanics [51].

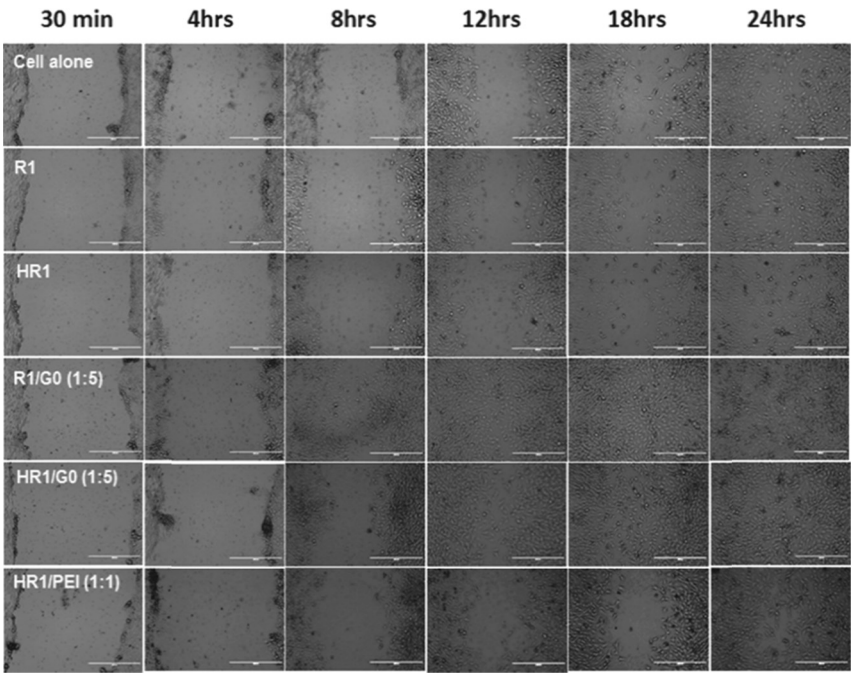

Fig. 2. *In vitro* scratch migration assay: Both *R1*/G0 and *HR1*/G0 at the weight ratio of 1:5 revealed the faster cell migration than *pDNA* alone and PEI polyplexes. The wt ratio of *pDNA*/polymer was expressed as (wt:wt).

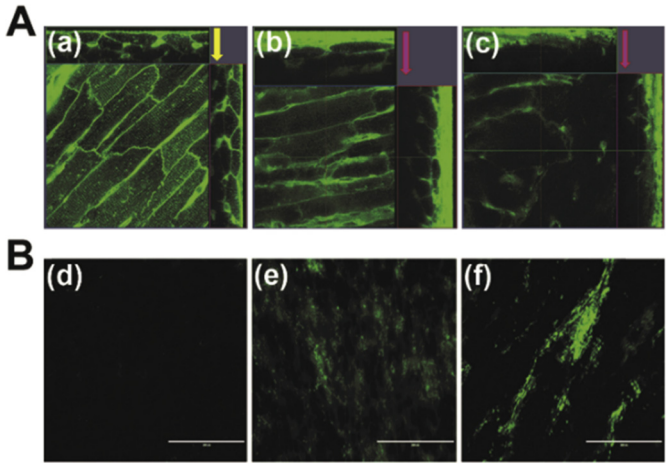

Fig. 3. A) Representative *ex vivo* 3D scanning confocal microscope image stacks labeled with WGA (green) in rat hearts. (a) normal; Myocytes are straightly aligned. (b) border zone of the infarct in LV (LVb); Myocyte structure appears irregular. (c) central fibrotic zone of the infarct in LV (LVf) on 1 wk after IR injury; Myocyte structure is nearly distorted. **B)** *in vivo* distribution pattern of different polymeric delivery carriers in the frozen sections of rat heart tissues on 48 h after intramyocardial injections. (d) *pGFP* alone. (e) *pGFP*/PAM-ABP G0 polyplexes. (f) *pGFP*/PEI polyplexes.

Compared with the I/R group, the 100 μg *HR1*/G0 polyplex group demonstrated qualitative and quantitative reversal of RWMA in most pathologic segments of hearts at 1 wk and 4 wks post-infarct, implying that it augments beneficial cardiac remodeling, confirming at a subdivisional functional level (Fig. 4B). Moreover, the 100 μg *HR1*/G0 polyplex group demonstrated the sustained functional improvement than I/R group and 200 μg *HR1*/PEI polyplex group on 4 weeks after MI (Fig. 4C). The *HR1* alone group showed a trend toward delayed increases of EF at 4 wks after I/R injury, but it was not significant. These suggest a promising therapeutic potential of human Relaxin gene therapy delivered by bioreducible dendrimer polymer for early phase clinical trials in MI.

Cardiac output (CO), the amount of blood that the heart pumps each minute, is obtained by multiplying stroke volume (SV) by heart rate (CO = SV × heart rate) and cardiac index (CI) by dividing CO by body surface area (BSA) (CI = CO/BSA) [52]. A low CO can reduce the delivery of oxygen and nutrients to other organs of the body, leading to failure of other organs. There was no significant difference in heart rate between the groups in this study (data not shown). In the comparable heart rate per minute, the 100 μg *HR1*/G0 group and 200 μg *HR1*/PEI polyplex group showed the enhanced stroke volume as well as cardiac output, up to the level of sham thoracotomy group in 1 wk after MI (Fig. 4D). Interestingly, both polymeric delivery system (G0 PAM-ABP and PEI) demonstrated improved cardiac hemodynamic function on 1 wk after I/R injury, compared with 200 μg *HR1* alone as well as I/R group. However, this hemodynamic functional improvement was maintained only in the 100 μg *HR1*/G0 polyplex group on 4 wks after MI than I/R, 200 μg *HR1* alone, and 200 μg *HR1*/PEI polyplex group (Fig. 4D). Altogether, the sustained improvement of SV and CO in 100 μg *HR1*/G0 polyplex group elucidates the beneficial functional efficacy of our bioreducible dendrimer delivery system. In clinics, inotropes and vasopressors were infused to improve CI including heart failure after MI. Because the BSA was comparable between the groups in this study (data not shown), the increases in SV and CO of 100 μg *HR1*/G0 polyplexes group can reflect improvement of CI during post-infarct cardiac remodeling. In addition, excess LV mass is associated with a cluster of geometric and functional abnormalities in heart [53]. Therefore, left ventricular hypertrophy (LVH), assessed by echocardiographic LV mass index is an independent predictor of incident HF, even irrespective of underlying LV systolic dysfunction, MI, and CV risk factors [53]. Eventually, the 100 μg *HR1*/G0 polyplexes group demonstrated well preserved LV mass in both end-diastolic and end-systolic phase and LV mass index than excess LV mass index of other treatment groups and I/R group (data not shown), which may predict less post-infarct co-morbidity, such as HF, after the treatment of 100 μg *HR1*/G0 polyplex system.

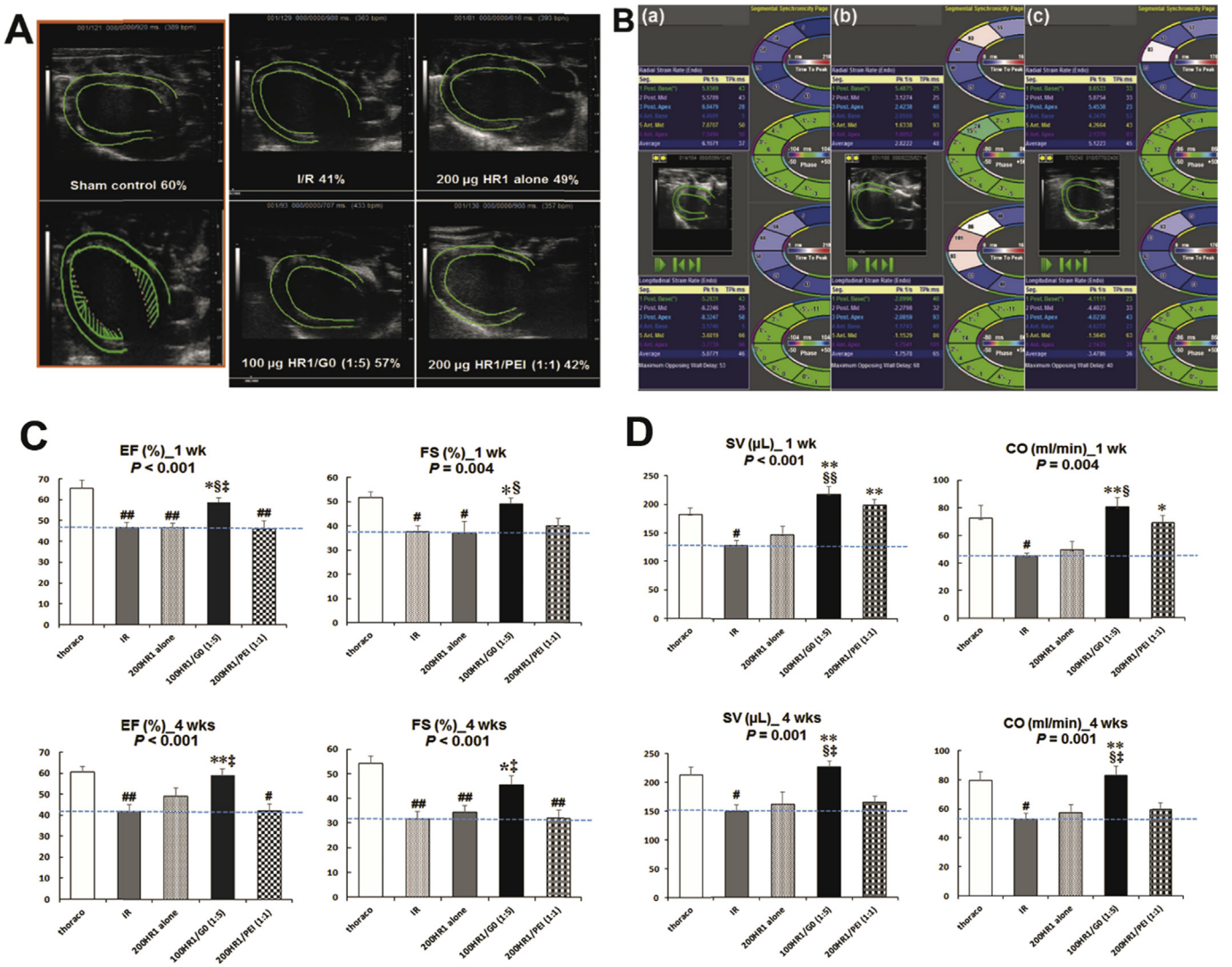

Fig. 4. A) Representative frames of 2D TTE image of the parasternal long-axis view on 1 wk after MI; measurement of ejection fraction (EF, %) by the Speckle Tracking Echocardiography (STE). **B)** evaluation of regional wall motion abnormality (RWMA) by strain rate on 1 wk after I/R injury; (a) sham control group. (b) I/R group. (c) 100 μg *HR1*/G0 polyplex group showed dramatic reversal of RWMA in LV wall after MI. **C)** systolic LV function by ejection fraction (EF) and fractional shortening (FS) and **D)** hemodynamic heart function during post-infarct cardiac remodeling 1 wk and 4 wks after I/R injury of MI. The stroke volume (SV) and cardiac output (CO). Expressed as the mean ± SEM, $n = 7–9$ per group. ##$P < 0.01$ vs sham thoracotomy, #$P < 0.05$ vs sham thoracotomy, **$P < 0.01$ vs I/R, *$P < 0.05$ vs I/R, §§$P < 0.01$ vs 200 *HR1* alone, §$P < 0.05$ vs 200 *HR1* alone, ‡$P < 0.05$ vs 200 *HR1*/PEI polyplex group.

3.4. *HR1* delivery enhances hemodynamic function of pLAD coronary artery

Recent advances in an echocardiographic diagnostic imaging tool made possible to evaluate the function of coronary artery [54,55]. In addition to the sustained improvement of representative systolic functional parameter (LV EF), we set out whether the *HR1*/G0 delivery exerts beneficial hemodynamic effects especially on the infarct-related proximal LAD (pLAD) coronary artery itself. To address this question, we focused on the time-dependent quantitative measurement of function and geometry of pLAD coronary artery using Doppler TTE. On 1 wk and 4 wks after I/R injury, the diameter and hemodynamic function of pLAD were not statistically different in between *HR1* alone group and 100 μg *HR1*/G0 polyplex group (Fig. 5a,b). There were no significant differences in mean velocity and peak velocity (mm/s) of pLAD between groups (data not shown). Because flow velocity varies during ejection in a pulsative system, like the cardiovascular system, in dividual velocities of the Doppler spectrum must be integrated to measure the total volume of flow during a given ejection period [52]. The sum of velocities is called the velocity time integral (VTI). However, the VTI and SV of coronary artery and coronary artery output were significantly enhanced only in 100 μg *HR1*/G0 polyplex group, up to the comparable level of thoracotomy control group, than I/R group in both 1 wk and 4 wks after MI (Fig. 5a,b). MI is caused by the occlusion of coronary artery. In the *HR1* gene therapy delivered by bioreducible dendrimer polymer, the anatomic and hemodynamic recovery of infarct-related pLAD coronary artery itself casts a pathophysiologically and clinically important prospect.

3.5. *HR1* delivery preserves LV geometry

During the cardiac remodeling followed by I/R injury of MI, the dimension of LV was dilated and the thickness of LV wall was thinned (Fig. 6A–C). Compared with on 1 wk after I/R injury, the preserved geometric effects of 100 μg *HR1*/G0 polyplex group on LV

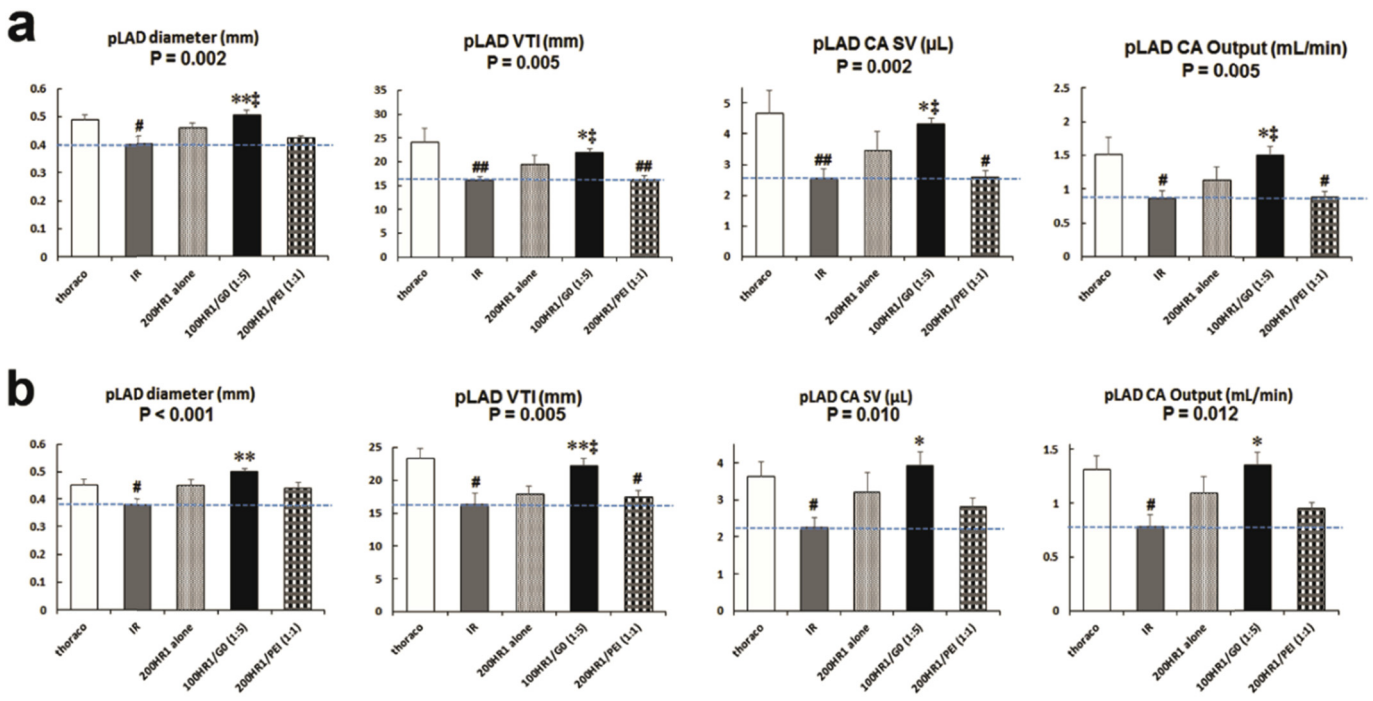

Fig. 5. The measurement of diameter and hemodynamic parameters of pLAD, infarct-related coronary artery by Doppler echocardiography on 1 wk (a) and 4 wks (b) after MI. Stroke volume of coronary artery (CA SV), blood volume output of coronary artery per min (CA Output), and velocity time integral (VTI). Expressed as the mean ± SEM, $n = 7–9$ per group. ##$P < 0.01$ vs sham thoracotomy, #$P < 0.05$ vs sham thoracotomy, **$P < 0.01$ vs I/R, *$P < 0.05$ vs I/R, ‡$P < 0.05$ vs 200 *HR1*/PEI polyplex group.

was prominent on 4 wks after I/R injury. There were no significant differences in the thickness of anterior wall and posterior of LV between group on 1 wk after MI. The *HR1* alone group as well as 100 μg *HR1*/G0 polyplex group showed better effects on the thickness of interventricular septum (IVS) on 4 wks after I/R than 100 μg *HR1*/PEI polyplex group and I/R group (Fig. 6C). Furthermore, only 100 μg *HR1*/G0 polyplex group demonstrated less dialated dimension of LV and less thinner thickness of anterior wall and posterior of LV than I/R group on 4 wks after I/R injury of MI (Fig. 6C). These LV geometric findings of *HR1*/G0 polyplexes group are closely related to the functional and hemodynamic improvements during post-infarct cardiac remodeling.

3.6. *HR1* effects on cardiac ECM composition

The ECM, forming bioactive polymers is composed of collagens and elastic fibers embedded in a viscoelastic gel, such as proteoglycans, hyaluronan, and glycoproteins [18]. Collagen is predominant in many cardiac ECM components. The subtype of collagen type I, a fibrillar collagen provides tensile strength and type III, an elastic collagen is most abundant in the cardiac ECM [6]. With replacing dead myocytes, collagen I is a representative cardiac ECM protein forming a fibrotic scar [15]. On 4 wks after MI in rat hearts, I/R, 200 μg *HR1* alone, and 200 μg *HR1*/PEI polyplex group showed remarkable accumulations in fibrotic cardiac ECM composition, such as collagen I, III, fibronectin, and elastin (Fig. 7). This prominent anti-fibrotic effect of *HR1* delivered by G0 PAM-ABP dendrimer on post-infarct cardiac remodeling may unravel the unmet need against fibrosis in diverse chronic diseases. This histopathologic analysis of cardiac ECM compositions provides the deeper understanding for the functional, hemodynamic, and geometric therapeutic efficacy of *HR1* delivered by bioreducible G0 polymer delivery system.

4. Discussion

Because cells utilize oxygen as the source of energy under the physiologic condition, the hypoxic injury causes functional loss and eventually pathologic fibrosis in heart, brain, liver, muscle, and solid tumors [56–60]. Gene delivery system working under hypoxia has major advantages that side-effects of gene therapy in normal tissues is reduced whereas the efficiency of gene therapy is selectively activated in the hypoxic damaged tissues. The final common pathway of oxygen signaling is the HRE promoter of effector genes [49,61]. The loss of the transcriptional HRE in the vascular endothelial growth factor (VEGF) promoter reported adult-onset progressive motor neuron degeneration in mice with neuropathological features reminiscent of amyotrophic lateral sclerosis in humans [57]. The multicopy of HRE has been considered as a potential candidates for diagnostic and therapeutic applications [62,63]. In human colon carcinoma HCT116 cells, gene activation levels mediated by HRE showed a linear correlation with an increase of HRE copy number and a saturation effect with more than 6 or 8 copies of an HRE [63]. However, the optimal HRE copy number for therapeutic genes was not determined in the diverse diseases yet [58]. In our study, the insertion of 12 copies of HRE showed enhanced *in vitro* transfection efficiency in both hypoxia and normoxia condition than without HRE insert (Fig. 1c).

In the *in vitro* results, G1 polyplexes with higher Zeta potential showed increased transfection efficiency than G0 polyplexes (at the wt/wt ratio of 5). In cardiac gene therapy, the compact cardiac ECM filled with negatively charged molecules, such as glycosaminoglycan and proteoglycan has been considered as a major hurdle of positively charged delivery system. To circumvent this problem, neutrally charged particles or negative charged naked pDNA or RNA itself have been explored. Proton-sponge polymers, including PAMAM and PEI exhibit p*K*a values between physiological and lysosomal pH, causing osmotic swelling and rupture of the

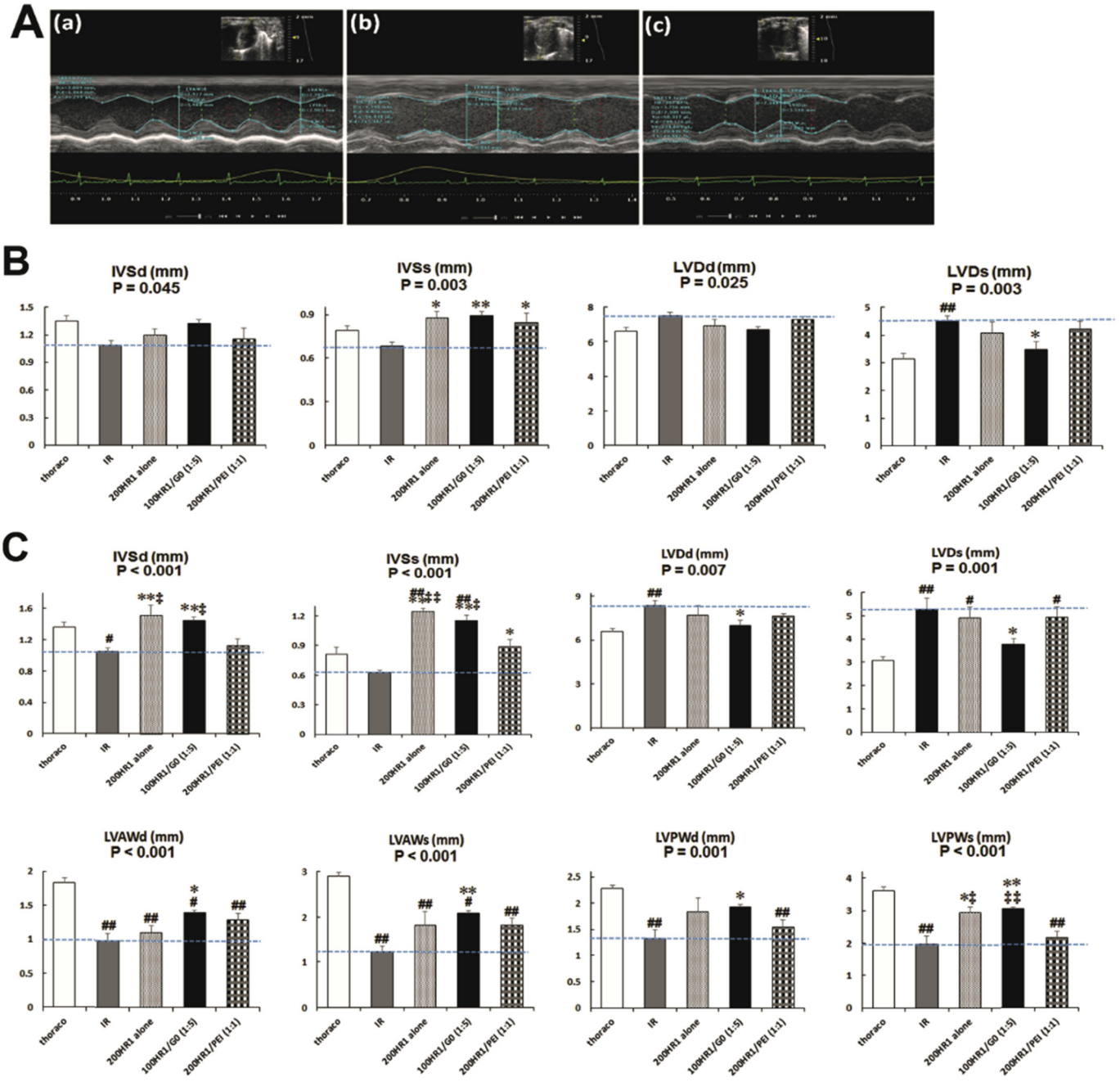

Fig. 6. **(A)** Representative M-mode echocardiograms at the mid-ventricular level of the parasternal long-axis view of 2D echocardiographic guidance on 1 wk after I/R injury; differences in the dimension and wall thickness of LV between (a) sham control group, (b) I/R group, and (c) 100 μg/G0 polyplex group. Assessment of cardiac geometry on 1 wk **(B)** and 4 wks **(C)** after MI. The thickness of interventricular septum (IVS), dimension of LV (LVD), thickness of anterior wall of LV (LVAW), and posterior wall of LV (LVPW) during diastole (d) and systole (s). Expressed as the mean ± SEM, $n = 7–9$ per group. ##$P < 0.01$ vs sham thoracotomy, #$P < 0.05$ vs sham thoracotomy, **$P < 0.01$ vs I/R, *$P < 0.05$ vs I/R, ‡‡$P < 0.01$ vs 200 *HR1*/PEI polyplex group, ‡$P < 0.05$ vs 200 *HR1*/PEI polyplex group.

endosome membrane, which releases of the polyplexes into the cytosol [40,64]. And, the application of dendrimer reported the higher attachment and prolonged retention of therapeutics in the ECM. To choose the better delivery system *in vivo*, we preformed the *in vivo* pilot study of *HR1*/polymer polyexes (with 50 μg or 100 μg for *HR1* pDNA) using *HR1*/ABP, *HR1*/G0, and *HR1*/G1 in 40-min I/R injury after 1 wk and 3 wks after MI in rat hearts (each n = 2) (data not shown). We can summarize results of the pilot study; First, *HR1*/G0 polyplexes showed significantly higher LV EF than *HR1*/G1 polyplexes, *HR1*/ABP polyplexes, and *HR1*/PEI polyplexes in 1 wk after MI. Second, dose-dependent (100 μg > 50 μg of *HR1* amount) functional improvement was observed irrelevant to the polymer type in 1 wk after MI. Third, 50 μg *HR1*/G0 polyplexes revealed delayed functional improvement in 4 wks after MI. Fourth, 100 μg *HR1*/G0 polyplexes revealed early and sustained functional improvement in both 1 wk and 4 wks after MI. Based on the results of this pilot study, we selected the PAM-ABP G0 polymer for the *HR1* delivery (*HR1*/G0) and the 100 μg of *HR1* amount for the therapeutic application in rat MI model.

Human and higher primates have three *RLX* genes, designated as *H1*, *H2*, and *H3 RLX*. The H2 RLX protein (or RLX-1 in rodents) is the major circulating and stored form of RLX. In failing atria, the

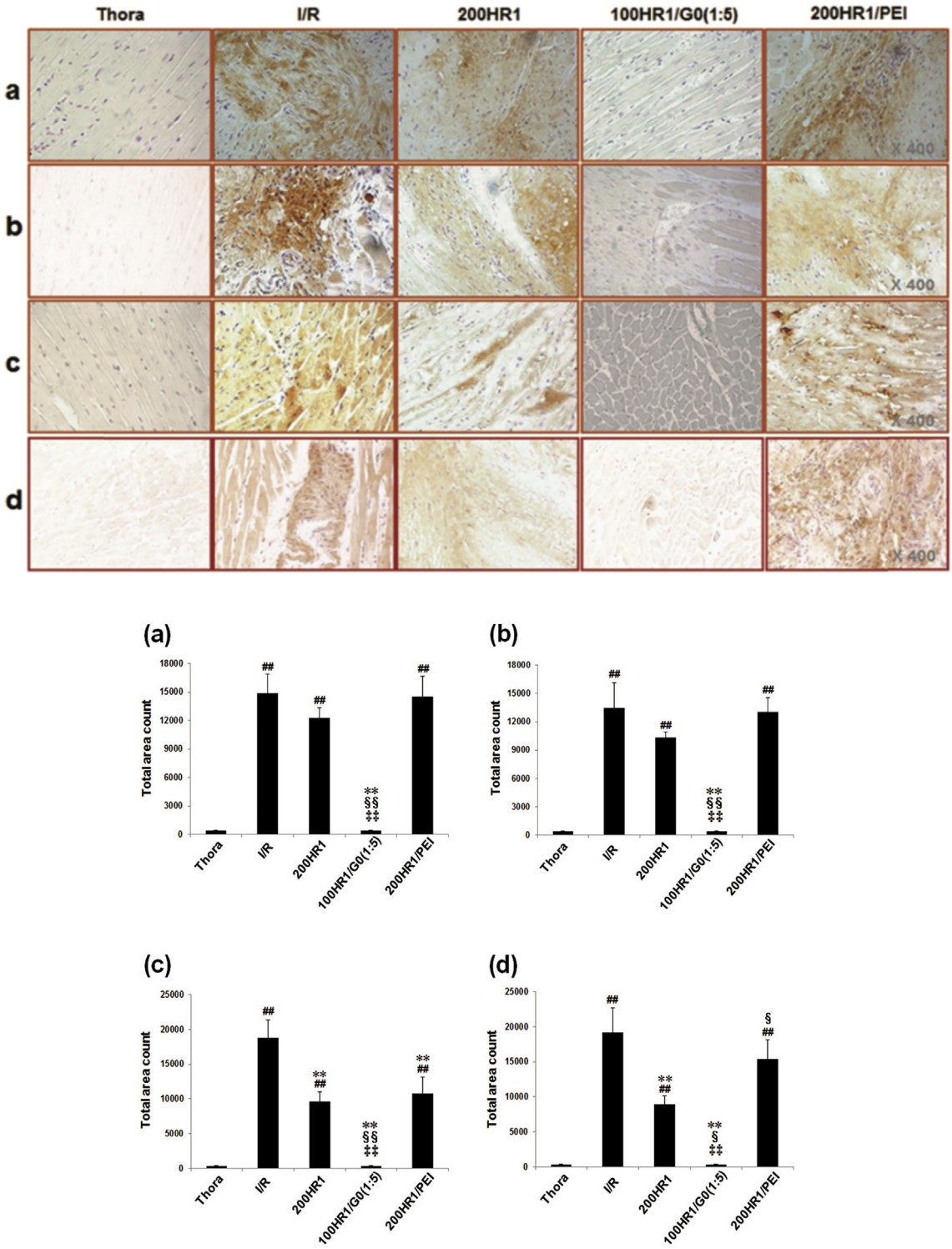

Fig. 7. Representative IHC staining images and quantitative analysis of cardiac ECM compositions in the LVb from each group on 4 wks after I/R injury (×400). (a) Collagen I. (b) Collagen III. (c) fibronectin. (d) elastin. Expressed as the mean ± SD, n = 7–9 per group. ##P < 0.001 vs sham thoracotomy, **P < 0.001 vs I/R, §§P < 0.001 vs 200 *HR1* alone, §P < 0.01 vs 200 *HR1* alone, ‡‡P < 0.001 vs 200 *HR1*/PEI polyplex group.

significant down-regulation of RXFP1, a receptor for RLX2 expression was observed compared with non-failing atria [65]. At first, it was considered that RLX exerts remarkable positive inotropy in atria but not in ventricles of rats, due to the lack of a relevant RXFP1 receptor on ventricular myocytes [65]. However, after resection of the atria in the isolated whole heart preparation, the purely dose-dependent chronotropic action of RLX in remained ventricles was still observed, implying that RLX acts on both the atrial and ventricular pacemaker to increase heart rate [66,67]. Chronic HF patients showed increased myocardial *RLX* gene expression and plasma RLX concentration in proportion to the stage of heart failure, suggesting that RLX may regulate cardiovascular function and

structure by autocrine and paracrine mechanisms [23,65,68]. In addition, an elevated left ventricular end-diastolic pressure (LVEDP) was reported to cause prominent up-regulation of *RLX* gene expression [68]. A nanomolar range of synthetic and recombinant human RLX protein (rhRLX) showed chronotropic and inotropic effects in rat hearts [29,67]. Also, rhRLX at 10 nM increased the concentration of atrial natriuretic peptide (ANP) in the coronary venous effluent [67]. Also, increases in cardiac output and global arterial compliance as well as reduced systemic vascular resistance were considered effects of RLX, especially during pregnancy. In our results, we speculate that the favorable modulation against cardiac myofibroblasts will cause less fibrotic scar tissue and provide more abundant healthy myocytes reflected on cardiac ECM composition. Diverse beneficial therapeutic effects of rhRLX in heart propose that *HR* gene therapy is a promising candidate for the diverse cardiovascular diseases.

The post-MI hearts are followed by sequential hemodynamic changes in patients. The congestive heart failure (CHF) is the most common complication after MI, explaining the 25% of post-MI comorbidity [3]. CHF is classified as a High-output and low-output. Without any affect on heart rate per min, the improved stroke volume and cardiac output assumed to be the beneficial therapeutic efficacy of *HR1* delivery system. In isolated and perfused hearts of guinea-pig and rat, the nanomolar concentrations of RLX hormone caused a concentration-dependent increase in coronary artery blood flow via a nitric oxide (NO) pathway, independent of heart rate, which was 50–500 fold more potent than the endothelium-dependent vasodilator, acetylcholine and the endothelium-independent vasodilator, sodium nitroprusside [26]. We first report this unrevealed hemodynamic impacts of *HR1* delivery system during post-infarct cardiac remodeling, highlighted in proximal LAD, infarct-related artery. In our study, *HR1*/G0 delivery system was able to improve myocardial perfusion by an increase in coronary blood flow as well as a decrease of cardiac load and systemic blood pressure. These several hemodynamic effects of RLX is presumed to be the circulatory adaptations during pregnancy.

Above all, *in vivo* administration of *HR1*/G0 polyplexes demonstrated favorable anti-fibrotic features of cardiac ECM composition, such as collagen I, III, fibronectin, and elastin. Overall, *HR1* gene therapy delivered by a bioreducible PAM-ABP G0 polymer would provide an advanced therapy for diverse cardiovascular applications with promising insight into favorable post-infarct cardiac remodeling, especially focused on hemodynamic improvement of infarct-related coronary artery and favorable modulation of cardiac ECM composition.

This study has some limitations. First, Heart demonstrates heterogeneous characteristics of myocardial remodeling at heart failure stage of different cardiac diseases [12]. *RLX M1* (equivalent to the *human RLX H2 gene*) gene knockout male mice developed age-related cardiac fibrosis, atrial hypertrophy, ventricular stiffening, and diastolic dysfunction, suggesting an important role as an intrinsic regulator of collagen turnover [24]. The ability of H2 RLX to inhibit collagen deposition and accumulation has been reported in many *in vivo* experiments [17,69]. However, we incompletely understand the cellular and molecular mechanisms necessary to produce a healthy ECM with sufficient tissue strength, function, and elasticity, against excessive deposition of fibrotic ECM [16,18,70]. Second, the effects of RLX has been studied with the receptors as the center [71,72]. Dschietzig T. et al. first demonstrated that upregulated expression of H1 and H2 RLX gene in the heart and vessels of patients with congestive HF was correlated with the severity of HF [68,73]. However, most investigations have conducted to examine H2 RLX. Very little is known of specific binding sites for other RLX family peptides, including H1 RLX. We don't know yet how much portion of H1 RLX can work by RXFP1, relaxin/insulin-like peptide family receptor 1, which is identified in both female and male reproductive tissues, the brain and numerous nonreproductive issues such as heart, kidney, and lung. To understand the effects of *HR1* gene therapy, correlation with receptor protein as well as comparison with *HR2* gene are needed in future. Third, in the *in vitro* scratch assay, we assumed that *HR1* delivered by bioreducible dendrimer polymer has stimulatory effects on cell migration by cell interaction with ECM and cell–cell interactions and exerts *in vivo* improved therapeutic efficacy during wound healing after MI, than *pDNA* alone and PEI polyplexes. However, this data of fibroblast cell alone is insufficient to translate into favorable *in vivo* correlation. In consideration of ECM, cross-talk between other cells and cytokines must be considered. Fourth, in post-MI cardiac remodeling, the slippage of myocytes occurs (Fig. 3a) [50]. The exogenous recombinant RLX has a potent anti-fibrotic effect on the ECM of diseased tissues, while not influencing the ECM of normal tissue [21,28,69]. Therefore, the beneficial effects of *HR1* gene therapy were speculated on enhanced myocyte survival, pro-angiogenesis, and anti-apoptosis. But, we didn't evaluate histopathology, instead of evaluation of geometric, hemodynamic, and ECM composition. Fifth, in our previous study of Erythropoietin gene therapy, it showed the suppression of pro-fibrotic Angiotensin II and TGF-β expression in the border zone of infarct as well as in the remote non-infarcted areas, such as atrium, septum, and right ventricle after MI [1]. To understand underlying mechanism of RLX, diverse molecular mechanism and cytokines have been discussed [71]. However, the circulating or tissue level of RLX expression was not measured to support diverse beneficial effects of *HR1* gene therapy in this study.

5. Conclusion

In this study, we constructed anti-fibrotic and cardioprotective *HR1* gene delivered by a bioreducible dendrimer polymer to induce favorable cardiac remodeling during cardiac ischemic cascade, especially after MI. We showed that *HR1*/G0 delivery system can be treated in MI, it allows improved myocardial systolic function, perfusion with hemodynamic contributions to overall and infarct-related coronary artery, and cardiac ECM recovery. This *HR1*/G0 delivery system suggests a potential for clinical translation. *HR1*/G0 delivery system maintained favorable post-infarct cardiac remodeling up to 1 month after MI. Future follow-up studies will be needed to evaluate the molecular mechanisms of *HR1*/G0 delivery system and to elucidate therapeutic efficacy on the infarct-related as well as the remote non-infarcted sites over a longer follow-up duration. Nonetheless, this study highlights the advanced effects of modified antifibrotic gene with optimal polymeric carrier in order to recover cardiac function and nature followed by MI.

Acknowledgments

This work was supported by grants from the National Research Foundation of Korea (2015R1A2A1A13027811 and 2013M3A9D3045879 ; Dr. C-O Yun) and the University of Utah Small Animal Ultrasound Core Facility in addition to the NIH National Center for Research through Award Number 1S10RR027506-01A01. The authors declare no competing financial interests. Hadi Javan, Christin Schaaf, and Kevin Whitehead M.D. guided and provided advices for TTE. Jaesung Kim and Il-Kyu Choi gave advices to construct the *pDNA* modification. Kihoon Nam synthesized our bioreducible polymers.

Appendix A. Supplementary data

Supplementary data related to this article can be found at http://dx.doi.org/10.1016/j.biomaterials.2016.04.025.

References

[1] Y. Lee, A.N. McGinn, C.D. Olsen, K. Nam, M. Lee, S.K. Shin, et al., Human erythropoietin gene delivery for cardiac remodeling of myocardial infarction in rats, J. Control Release 171 (2013) 24–32.
[2] D. Lloyd-Jones, R.J. Adams, T.M. Brown, M. Carnethon, S. Dai, G. De Simone, et al., Heart disease and stroke statistics–2010 update: a report from the american heart association, Circulation 121 (2010) e46–e215.
[3] D.M. Yellon, D.J. Hausenloy, Myocardial reperfusion injury, N. Engl. J. Med. 357 (2007) 1121–1135.
[4] T.A. Gaziano, A. Bitton, S. Anand, S. Abrahams-Gessel, A. Murphy, Growing epidemic of coronary heart disease in low- and middle-income countries, Curr. Probl. Cardiol. 35 (2010) 72–115.
[5] C.D. Mathers, D. Loncar, Projections of global mortality and burden of disease from 2002 to 2030, PLoS Med. 3 (2006) e442.
[6] J.J. Gajarsa, R.A. Kloner, Left ventricular remodeling in the post-infarction heart: a review of cellular, molecular mechanisms, and therapeutic modalities, Heart Fail Rev. 16 (2011) 13–21.
[7] K. Thygesen, J.S. Alpert, A.S. Jaffe, M.L. Simoons, B.R. Chaitman, H.D. White, et al., Third universal definition of myocardial infarction, Circulation 126 (2012) 2020–2035.
[8] P.A. Heidenreich, J.G. Trogdon, O.A. Khavjou, J. Butler, K. Dracup, M.D. Ezekowitz, et al., Forecasting the future of cardiovascular disease in the united states: a policy statement from the american heart association, Circulation 123 (2011) 933–944.
[9] S. Windecker, J.J. Bax, A. Myat, G.W. Stone, M.S. Marber, Future treatment strategies in st-segment elevation myocardial infarction, Lancet 382 (2013) 644–657.
[10] M. Dobaczewski, C. Gonzalez-Quesada, N.G. Frangogiannis, The extracellular matrix as a modulator of the inflammatory and reparative response following myocardial infarction, J. Mol. Cell Cardiol. 48 (2010) 504–511.
[11] E.A. Liehn, O. Postea, A. Curaj, N. Marx, Repair after myocardial infarction, between fantasy and reality: the role of chemokines, J. Am. Coll. Cardiol. 58 (2011) 2357–2362.
[12] A. Gonzalez, S. Ravassa, J. Beaumont, B. Lopez, J. Diez, New targets to treat the structural remodeling of the myocardium, J. Am. Coll. Cardiol. 58 (2011) 1833–1843.
[13] F.G. Spinale, M.R. Zile, Integrating the myocardial matrix into heart failure recognition and management, Circ. Res. 113 (2013) 725–738.
[14] E.C. Goldsmith, A.D. Bradshaw, F.G. Spinale, Cellular mechanisms of tissue fibrosis. 2. Contributory pathways leading to myocardial fibrosis: moving beyond collagen expression, Am. J. Physiol. Cell Physiol. 304 (2013) C393–C402.
[15] J.S. Burchfield, M. Xie, J.A. Hill, Pathological ventricular remodeling: mechanisms: Part 1 of 2, Circulation 128 (2013) 388–400.
[16] T.A. Wynn, Cellular and molecular mechanisms of fibrosis, J. Pathol. 214 (2008) 199–210.
[17] X.J. Du, Q. Xu, E. Lekgabe, X.M. Gao, H. Kiriazis, X.L. Moore, et al., Reversal of cardiac fibrosis and related dysfunction by relaxin, Ann. N. Y. Acad. Sci. 1160 (2009) 278–284.
[18] T.N. Wight, S. Potter-Perigo, The extracellular matrix: an active or passive player in fibrosis? Am. J. Physiol. Gastrointest. Liver Physiol. 301 (2011) G950–G955.
[19] S.C. Tyagi, Extracellular matrix dynamics in heart failure: a prospect for gene therapy, J. Cell Biochem. 68 (1998) 403–410.
[20] B. Hinz, S.H. Phan, V.J. Thannickal, M. Prunotto, A. Desmouliere, J. Varga, et al., Recent developments in myofibroblast biology: paradigms for connective tissue remodeling, Am. J. Pathol. 180 (2012) 1340–1355.
[21] I.K. Choi, R. Strauss, M. Richter, C.O. Yun, A. Lieber, Strategies to increase drug penetration in solid tumors, Front. Oncol. 3 (2013) 193.
[22] F. Hisaw, Experimental relaxation of the pubic ligament of the guinea pig, Proc. Soc. Exp. Biol. Med. 23 (1926) 661–663.
[23] V. Cernaro, A. Lacquaniti, R. Lupica, A. Buemi, D. Trimboli, G. Giorgianni, et al., Relaxin: new pathophysiological aspects and pharmacological perspectives for an old protein, Med. Res. Rev. 34 (2014) 77–105.
[24] X.J. Du, C.S. Samuel, X.M. Gao, L. Zhao, L.J. Parry, G.W. Tregear, Increased myocardial collagen and ventricular diastolic dysfunction in relaxin deficient mice: a gender-specific phenotype, Cardiovasc. Res. 57 (2003) 395–404.
[25] X.J. Du, R.A. Bathgate, C.S. Samuel, A.M. Dart, R.J. Summers, Cardiovascular effects of relaxin: from basic science to clinical therapy, Nat. Rev. Cardiol. 7 (2010) 48–58.
[26] T. Bani-Sacchi, M. Bigazzi, D. Bani, P.F. Mannaioni, E. Masini, Relaxin-induced increased coronary flow through stimulation of nitric oxide production, Br. J. Pharmacol. 116 (1995) 1589–1594.
[27] T.D. Hewitson, C. Zhao, B. Wigg, S.W. Lee, E.R. Simpson, W.C. Boon, et al., Relaxin and castration in male mice protect from, but testosterone exacerbates, age-related cardiac and renal fibrosis, whereas estrogens are an independent determinant of organ size, Endocrinology 153 (2012) 188–199.
[28] J.H. Kim, Y.S. Lee, H. Kim, J.H. Huang, A.R. Yoon, C.O. Yun, Relaxin expression from tumor-targeting adenoviruses and its intratumoral spread, apoptosis induction, and efficacy, J. Natl. Cancer Inst. 98 (2006) 1482–1493.
[29] C.S. Samuel, X.J. Du, R.A. Bathgate, R.J. Summers, 'Relaxin' the stiffened heart and arteries: the therapeutic potential for relaxin in the treatment of cardiovascular disease, Pharmacol. Ther. 112 (2006) 529–552.
[30] C.S. Samuel, S. Cendrawan, X.M. Gao, Z. Ming, C. Zhao, H. Kiriazis, et al., Relaxin remodels fibrotic healing following myocardial infarction, Lab. Investig. 91 (2011) 675–690.
[31] C.S. Samuel, T.D. Hewitson, Y. Zhang, D.J. Kelly, Relaxin ameliorates fibrosis in experimental diabetic cardiomyopathy, Endocrinology 149 (2008) 3286–3293.
[32] J.R. Teerlink, G. Cotter, B.A. Davison, G.M. Felker, G. Filippatos, B.H. Greenberg, et al., Serelaxin, recombinant human relaxin-2, for treatment of acute heart failure (relax-ahf): a randomised, placebo-controlled trial, Lancet 381 (2013) 29–39.
[33] M. Metra, G. Cotter, B.A. Davison, G.M. Felker, G. Filippatos, B.H. Greenberg, et al., Effect of serelaxin on cardiac, renal, and hepatic biomarkers in the relaxin in acute heart failure (relax-ahf) development program: correlation with outcomes, J. Am. Coll. Cardiol. 61 (2013) 196–206.
[34] R.M. Kannan, E. Nance, S. Kannan, D.A. Tomalia, Emerging concepts in dendrimer-based nanomedicine: from design principles to clinical applications, J. Intern Med. 276 (2014) 579–617.
[35] D. Shcharbin, A. Shakhbazau, M. Bryszewska, Poly(amidoamine) dendrimer complexes as a platform for gene delivery, Expert Opin. Drug Deliv. 10 (2013) 1687–1698.
[36] R. Duncan, L. Izzo, Dendrimer biocompatibility and toxicity, Adv. Drug Deliv. Rev. 57 (2005) 2215–2237.
[37] U. Boas, P.M. Heegaard, Dendrimers in drug research, Chem. Soc. Rev. 33 (2004) 43–63.
[38] D.V. Sakharov, A.F. Jie, M.E. Bekkers, J.J. Emeis, D.C. Rijken, Polylysine as a vehicle for extracellular matrix-targeted local drug delivery, providing high accumulation and long-term retention within the vascular wall, Arterioscler. Thromb. Vasc. Biol. 21 (2001) 943–948.
[39] M. El-Sayed, M.F. Kiani, M.D. Naimark, A.H. Hikal, H. Ghandehari, Extravasation of poly(amidoamine) (pamam) dendrimers across microvascular network endothelium, Pharm. Res. 18 (2001) 23–28.
[40] D.W. Pack, A.S. Hoffman, S. Pun, P.S. Stayton, Design and development of polymers for gene delivery, Nat. Rev. Drug Discov. 4 (2005) 581–593.
[41] H.Y. Nam, K. Nam, M. Lee, S.W. Kim, D.A. Bull, Dendrimer type bio-reducible polymer for efficient gene delivery, J. Control Release 160 (2012) 592–600.
[42] Y. Lee, H.Y. Nam, J. Kim, M. Lee, J.W. Yockman, S.K. Shin, et al., Human erythropoietin gene delivery using an arginine-grafted bioreducible polymer system, Mol Ther. 20 (2012) 1360–1366.
[43] T.I. Kim, M. Ou, M. Lee, S.W. Kim, Arginine-grafted bioreducible poly(disulfide amine) for gene delivery systems, Biomaterials 30 (2009) 658–664.
[44] Y.S. Lee, S.W. Kim, Bioreducible polymers for therapeutic gene delivery, J. Control Release 190 (2014) 424–439.
[45] C.C. Liang, A.Y. Park, J.L. Guan, In vitro scratch assay: a convenient and inexpensive method for analysis of cell migration in vitro, Nat. Protoc. 2 (2007) 329–333.
[46] F.B. Sachse, N.S. Torres, E. Savio-Galimberti, T. Aiba, D.A. Kass, G.F. Tomaselli, et al., Subcellular structures and function of myocytes impaired during heart failure are restored by cardiac resynchronization therapy, Circ. Res. 110 (2012) 588–597.
[47] B.C. Schwab, G. Seemann, R.A. Lasher, N.S. Torres, E.M. Wulfers, M. Arp, et al., Quantitative analysis of cardiac tissue including fibroblasts using three-dimensional confocal microscopy and image reconstruction: towards a basis for electrophysiological modeling, IEEE Trans. Med. Imaging 32 (2013) 862–872.
[48] K. Ujino, M. Teragaki, T. Ota, T. Muro, H. Watanabe, M. Yoshiyama, et al., Novel method for assessing myocardial perfusion: visualization and measurement of intramyocardial coronary blood flow in the entire left ventricular wall using contrast enhanced, high frequency doppler echocardiography, Jpn. Heart J. 42 (2001) 101–113.
[49] T. Rhim, D.Y. Lee, M. Lee, Hypoxia as a target for tissue specific gene therapy, J. Control Release 172 (2013) 484–494.
[50] G. Olivetti, J.M. Capasso, E.H. Sonnenblick, P. Anversa, Side-to-side slippage of myocytes participates in ventricular wall remodeling acutely after myocardial infarction in rats, Circ. Res. 67 (1990) 23–34.
[51] T.H. Marwick, Measurement of strain and strain rate by echocardiography: ready for prime time? J. Am. Coll. Cardiol. 47 (2006) 1313–1327.
[52] J. Oh, J. Seward, A. Tajik, The Echo Manual, third ed., Lippincott Williams & Wilkins, 2006, pp. 59–79.
[53] G. de Simone, J.S. Gottdiener, M. Chinali, M.S. Maurer, Left ventricular mass predicts heart failure not related to previous myocardial infarction: the cardiovascular health study, Eur. Heart J. 29 (2008) 741–747.
[54] H.J. Youn, E. Foster, Demonstration of coronary artery flow using transthoracic doppler echocardiography, J. Am. Soc. Echocardiogr. 17 (2004) 178–185.
[55] Y.S. Lee, W.S. Joo, H.S. Kim, S.W. Kim, Human mesenchymal stem cell delivery system modulates ischemic cardiac remodeling with an increase of coronary artery blood flow, Mol Ther. 24 (2016) 805–811.
[56] S. Cannito, C. Paternostro, C. Busletta, C. Bocca, S. Colombatto, A. Miglietta, et al., Hypoxia, hypoxia-inducible factors and fibrogenesis in chronic liver diseases, Histol. Histopathol. 29 (2014) 33–44.

[57] B. Oosthuyse, L. Moons, E. Storkebaum, H. Beck, D. Nuyens, K. Brusselmans, et al., Deletion of the hypoxia-response element in the vascular endothelial growth factor promoter causes motor neuron degeneration, Nat. Genet. 28 (2001) 131–138.
[58] H. Ruan, J. Wang, L. Hu, C.S. Lin, K.R. Lamborn, D.F. Deen, Killing of brain tumor cells by hypoxia-responsive element mediated expression of bax, Neoplasia 1 (1999) 431–437.
[59] E.C. Toescu, Hypoxia response elements, Cell Calcium 36 (2004) 181–185.
[60] H. Hoppeler, M. Vogt, E.R. Weibel, M. Fluck, Response of skeletal muscle mitochondria to hypoxia, Exp. Physiol. 88 (2003) 109–119.
[61] R.H. Wenger, D.P. Stiehl, G. Camenisch, Integration of oxygen signaling at the consensus hre, Sci. STKE 2005 (2005) re12.
[62] J. Zhang, Q. Shi, X. Chen, P. Yang, C. Qi, H. Lu, et al., Hypoxia-regulated neurotrophin-3 expression by multicopy hypoxia response elements reduces apoptosis in pc12 cells, Int. J. Mol. Med. 30 (2012) 1173–1179.
[63] Y. Takeuchi, M. Inubushi, Y.N. Jin, C. Murai, A.B. Tsuji, H. Hata, et al., Detailed assessment of gene activation levels by multiple hypoxia-responsive elements under various hypoxic conditions, Ann. Nucl. Med. 28 (2014) 1011–1019.
[64] N. Daneshvar, R. Abdullah, F.T. Shamsabadi, C.W. How, M.A. Mh, P. Mehrbod, Pamam dendrimer roles in gene delivery methods and stem cell research, Cell Biol. Int. 37 (2013) 415–419.
[65] T. Dschietzig, K. Alexiou, H.T. Kinkel, G. Baumann, K. Matschke, K. Stangl, The positive inotropic effect of relaxin-2 in human atrial myocardium is preserved in end-stage heart failure: role of g(i)-phosphoinositide-3 kinase signaling, J. Card. Fail. 17 (2011) 158–166.
[66] G.R. Thomas, R. Vandlen, The purely chronotropic effects of relaxin in the rat isolated heart, J. Pharm. Pharmacol. 45 (1993) 927–928.
[67] K.P. Conrad, J. Novak, Emerging role of relaxin in renal and cardiovascular function, Am. J. Physiol. Regul. Integr. Comp. Physiol. 287 (2004) R250–R261.
[68] T. Dschietzig, C. Richter, C. Bartsch, M. Laule, F.P. Armbruster, G. Baumann, et al., The pregnancy hormone relaxin is a player in human heart failure, FASEB J. 15 (2001) 2187–2195.
[69] C.S. Samuel, Relaxin: antifibrotic properties and effects in models of disease, Clin. Med. Res. 3 (2005) 241–249.
[70] B.C. Berk, K. Fujiwara, S. Lehoux, Ecm remodeling in hypertensive heart disease, J. Clin. Investig. 117 (2007) 568–575.
[71] R.A. Bathgate, M.L. Halls, E.T. van der Westhuizen, G.E. Callander, M. Kocan, R.J. Summers, Relaxin family peptides and their receptors, Physiol. Rev. 93 (2013) 405–480.
[72] R.A. Bathgate, R. Ivell, B.M. Sanborn, O.D. Sherwood, R.J. Summers, International union of pharmacology lvii: recommendations for the nomenclature of receptors for relaxin family peptides, Pharmacol. Rev. 58 (2006) 7–31.
[73] C.S. Samuel, T.D. Hewitson, Relaxin in cardiovascular and renal disease, Kidney Int. 69 (2006) 1498–1502.